A Magnetic Microstirrer and Array for Microfluidic Mixing

Liang-Hsuan Lu, Kee Suk Ryu, and Chang Liu

***Abstract*—We report the development of a micromachined magnetic-bar micromixer for microscale fluid mixing in biological laboratory-on-a-chip applications. The mixer design is inspired by large scale magnetic bar mixers. A rotating magnetic field causes a single magnetic bar or an array of them to rotate rapidly within a fluid environment. A fabrication process of the magnetic bar mixer is developed. Results of fluid mixing in micro channels and chambers are investigated using experimental means and computer-aided fluid simulation. [729]**

***Index Terms*—Active mixer, magnetic actuation, microfluidics, mixer array.**

I. Introduction

MICROSCALE fluid mixing is crucial and challenging for microfluidic systems applications [1], [2]. Successful performance of on-chip biochemical analysis processes such as DNA hybridization and PCR amplification depend on rapid mixing of multiple fluid species.

Mixing comprises three mechanisms of mass transfer: molecular diffusion, eddy diffusion and bulk diffusion. On the macroscale, turbulence can generate large eddies and bulk diffusion dominate over molecular diffusion. On the microscale, however, molecular diffusion becomes more important while the eddy diffusion and the bulk diffusion components are limited under the low Reynolds number condition. Mixing at the microscale is governed by molecular diffusion and the speed of mixing is severely limited. Consequently, time inefficiency is the major problem with molecular diffusion [3].

Downscaling the channel dimension improves mixing efficiency for molecular diffusion. Mixing times below 100 μs with fast diffusion in nozzles of a few micrometers were reported [4], [5]. However, such a mixing scheme is achieved at the cost of large pressure drops and potential channel clogging. An alternative approach is to increase the interfacial area between two fluids. At the molecular level, the volume mixed at a given time t is

$$V = A\sqrt{Dt} \tag{1}$$

where A is the contact area between the fluids being mixed and D is the diffusion constant. For a given fluid volume, the mixing time is reduced when the area A increases.

In order to enhance the rate of fluid mixing, previous work has been dedicated to increase the contact area between two fluids. The reported approaches for rapid microscale mixing fall into two categories: passive mixing and active mixing. Passive mixing is typically accomplished by driving fluids through channels with delicate, fixed geometries. Repeated lamination and splitting of flows in 20- to 50-μm wide channels was used to increase the interfacial area and thus the mixing efficiency [6]–[8]. An alternative method is to apply the so-called "Lagrangian chaos" or "chaotic advection," which is based on the fact that chaotic and ergodic fluid pathlines can occur and disperse fluid species effectively, even in smooth and regular flow fields [9]. Three-dimensional chaotic mixing using serpentine and twisted channels have been achieved [10], [11]. However, one disadvantage of such mixing methods lies in the fact that, in order to develop strong chaotic advection, it is necessary to use complex three-dimensional microstructures. Recently, a passive mixer with bas-relief structures has also been demonstrated [12].

Active mixing, based on chaotic advection, is usually achieved by periodic perturbation of the flow fields. In such time-dependent two-dimensional flows, chaos can occur and be used to improve the efficiency of mixing. Several fluid actuation methods have been demonstrated, including heat convection [13], differential pressure [14]–[17], ultrasonic or piezoelectric actuation [18]–[21], vapor pneumatic power [22], [23], magnetic actuation [24], [25] and electrokinetic (EK) pressure [26]. One important advantage of the active mixers is that they can be activated on-demand. However, these require external power sources and hence are more complex to package and control. The performance of EK-based active mixing is also conjectured to be dependent on electrochemical properties of fluids. Further, some active mixing methods have been demonstrated to work well for channel mixing but not for mixing in reaction chambers.

II. Mixer Principle

In this paper, we present an active mixer employing micromagnetic rotating bar stirrers and arrays. The feasibility and potential usefulness of a magnetic micro actuator in a fluidic environment were first demonstrated by Judy, Zappe, and Muller [27]. It is conjectured that mechanical stirring in microchannels can generate bulk motion (circulation loops) in the flow, potentially reducing the time needed for pure diffusion. The micro-

Manuscript received July 23, 2001; revised March 3, 2002. This work was supported by the DARPA CompositeCAD program under Contract F30602-98-2-0178 (managed by Dr. A. Krishnan). Subject Editor T. Kenny.

L.-H. Lu and K. S. Ryu are with the Micro Actuators, Sensors and Systems Group, Micro and Nanotechnology Laboratory, University of Illinois at Urbana-Champaign Urbana, IL 61801 USA.

C. Liu is with the Micro and Nanotechnology Laboratory, University of Illinois at Urbana-Champaign, Urbana, IL 61801 USA (e-mail: changliu@uiuc.edu).

Digital Object Identifier 10.1109/JMEMS.2002.802899.

magnetic bar stirrer is a miniaturized mixer of the kind commonly found in chemistry laboratories (see Fig. 1). The centerpiece of the mixer is a rotating bar (rotor) made of a ferromagnetic material. When a rotating external magnetic field is applied, the rotor will magnetize and experience a torque through interaction between its internal magnetization and the external field. When the torque exceeds the friction force, the rotor will rotate following the external magnetic field. A hub provides a rotational axis and prevents the rotor from leaving the substrate.

A microstirrer offers a unique alternative approach to mixing. The new mixing principle provides the following performance characteristics and advantages.

1) Rapid mixing in a channel can be realized within the characteristic length of a stirrer bar.
2) The mixer array allows effective mixing in a larger reaction chamber for *sequential flow analysis*.
3) Magnetic actuation, applied externally, eliminates the need for tether wires and reduces the control complexity.
4) The mixer can be used for a wide variety of fluids with different electrochemical characteristics.

III. Theory and Design

Pertinent design parameters of the mixer include the length, width and thickness of the rotor, as well as the rotation speed of the mixer. The thickness of the beam affects the mixing efficiency and the actuation force. It is conjectured that the mixing efficiency will suffer if the rotor is too thin compared to the heights of the fluid chambers or channels. On the other hand, the thickness is limited by the fabrication method we use to realize the rotor. The design of the rotor thickness is therefore a compromise between fabrication requirements and mixing performance.

Optimization of the design of such a micromixer rotor is made difficult by the fact that the local flow field around the rotor is three-dimensional in nature and that the scale is microscopic. Neither theoretical studies nor computational tools for investigating the fluid flow at the length scale of interest are sufficient or readily available. In order to generate the initial design we looked to literature on macroscopic mixers. The geometry effects of macroscopic stirrers have been studied for applications in food, chemistry and material industries. For example, Patwardhan and Joshi conducted a detailed analysis of impeller blades in macroscale stirred mixing tanks [28]. Their studies revealed that the mixing time is dependent on the dimensions of the impeller and that the shortest mixing time was achieved when the ratio of the diameter of an impeller (analog to the stirrer bar length) to the vessel (analog to the channel width) equals 0.5. However, such studies only provide first-order guidance to our design since the micromixer rotor does not have complex three-dimensional curved surfaces for propulsion of fluids.

We used design principles of macroscopic mixers to guide the initial design. For a channel width of 750 μm, we designed the microstirrer bar with a span of 400 μm. For larger mixing volumes (i.e., for a mixing chamber), we designed arrays of smaller stirrers that cover the area of the entire chamber.

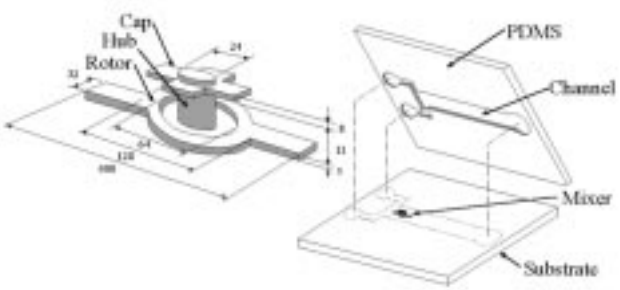

Fig. 1. Schematic diagram of a single microstirrer in the fluidic device. The rotating bar is prevented from leaving the substrate by a hub. Unit: μm.

The width of the rotor has a second-order effect on the performance. With increased width, the rotor inertia will increase and the friction with the supporting substrate will likely increase. However, due to the use of friction-reducing tips, the increase of friction is contributed only through the increased weight of the rotor but not the contact area. In our design, we use a width-to-length ratio of 0.1, a value typically found for commercial magnetic stirrers and a bar thickness of about 5 μm. The pertinent design variables of a single stirrer are labeled in Fig. 1.

IV. Development of Fabrication Process

In this section, we discuss the fabrication process for realizing individual mixers and for packaging the assembly of microchannels and mixers.

A. Fabrication of Micromixer

The developed surface-micromachining fabrication process of the stirrer is low temperature in nature and involves a minimal number of steps. The process, illustrated in Fig. 2, begins with 2-in glass wafers (Corning Pyrex 7740, Esco Products, Inc., Oak Ridge, NJ). Other substrates such as silicon wafer and hard polymer can also be used. First, a 200-Å-thick chromium thin film is deposited, followed by a 2000-Å-thick gold thin film. The Cr/Au films are then patterned as a precursor for making the hub [see Fig. 2(a)]. Next, a 1-μm-thick copper film is evaporated as the sacrificial layer [see Fig. 2(b)]. Dimples that are 2 μm on the side and 0.5 μm deep are patterned and etched in the copper film using a wet Cu etchant (DI: H_2O_2: acetic acid, 20:1:1). The etched dimple reserves the space for defining tips on the bottom of rotors [see Fig. 2(c)]. Such tips reduce the overall contact area between the rotor and the substrate and hence decrease the friction.

Subsequently, 10-μm-thick photoresist (AZ 4620) is spin-coated and patterned on top of the Cu layer. Care is taken to ensure there is no copper oxide on the surface. Rotors are then formed by selective electroplating. The thickness of the electroplated layer determines the thickness of the rotor (5 μm). Tips are formed at the bottom of the rotors by molding against the dimples [see Fig. 2(d)]. A second 10-mm-thick photoresist mask is used first to selectively remove the Cu seedlayer material and then serves as the electroplating mold for the hub. It provides spacing for the upcoming cap structure. Once the gold layer is selectively exposed, a 16-μm-tall hub is formed by electroplating Permalloy on top of the gold layer [see Fig. 2(f)]. A

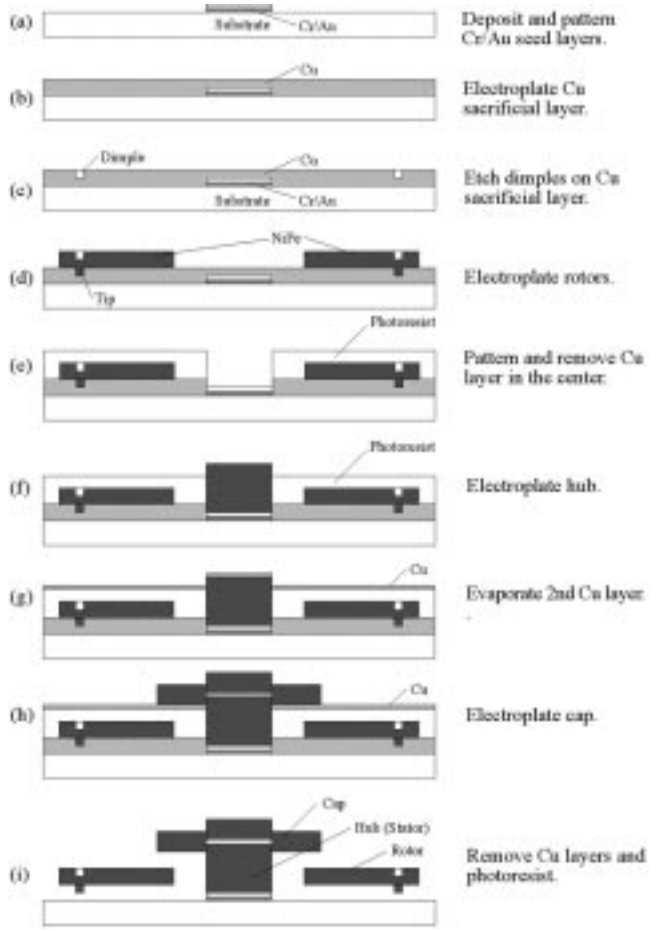

Fig. 2. Schematic illustration of the fabrication process of the microstirrer bar.

second Cu sacrificial layer (3000 Å thick) is evaporated over the hub and the photoresist layer [see Fig. 2(g)]. The cap is formed by electroplating selectively, to a height of 8 μm, on top of this new copper layer [see Fig. 2(h)]. We complete the stirrer by removing all copper sacrificial layers, allowing the rotor to move freely with respect to the hub.

The three-dimensional surface topography of a mixer array after release is shown in Fig. 3. The distance between two microstirrers is 500 μm and the overall height is 25 μm. Scanning electron micrographs of a single microstirrer and a 5×3 array are shown in Fig. 4. A 0.5-μm gap between the rotor and the substrate, defined by the tips, is shown in the inserted graph of Fig. 4.

B. Fabrication of Fluid Network

For our work we used a simple and straightforward approach to construct the fluid network. Namely, microfluidic devices are formed by bonding pieces made of polydimethylsiloxane (PDMS, DuPont Sylgard 184 Silicone Elastomer) onto glass wafers that contain built-in mixers (Fig. 1). The microfluidic network consists of two fluid inlets, an outlet and a T-channel (750 μm wide, 70 μm deep and 4 mm long).

There are other alternatives to fabricating the integrated channel/mixer assembly. For example, we believe it is possible to fabricate integrated microfluid channels using Parylene by extending a process first introduced in [29]. However, in this work we focus on the development of the mixer itself; therefore, we used the most straightforward fabrication technique to realize the fluid network.

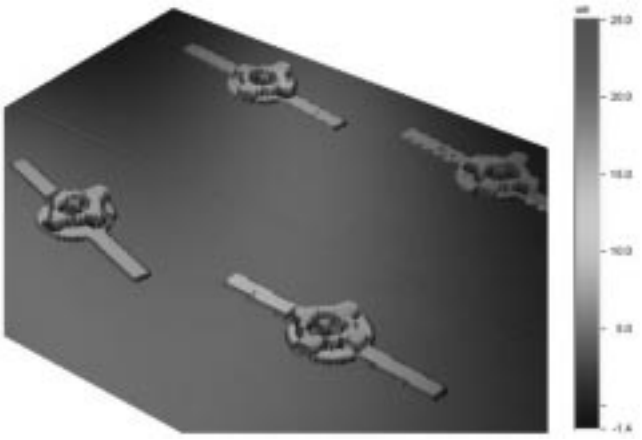

Fig. 3. 3D surface topology of a 2×2 mixer array measured by an optical profilometer (Veeco NT1000).

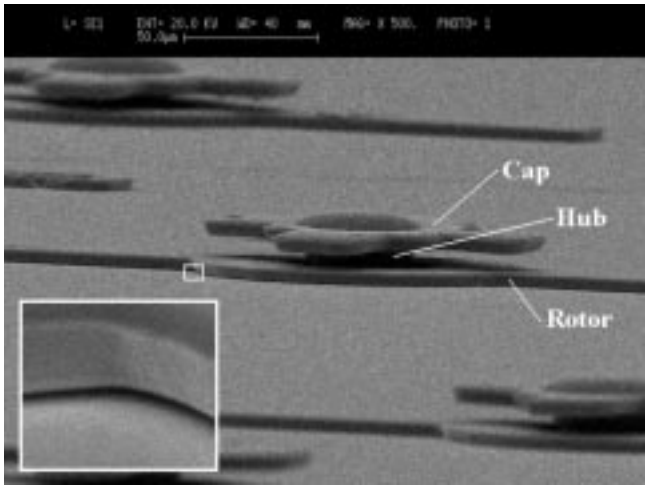

(a)

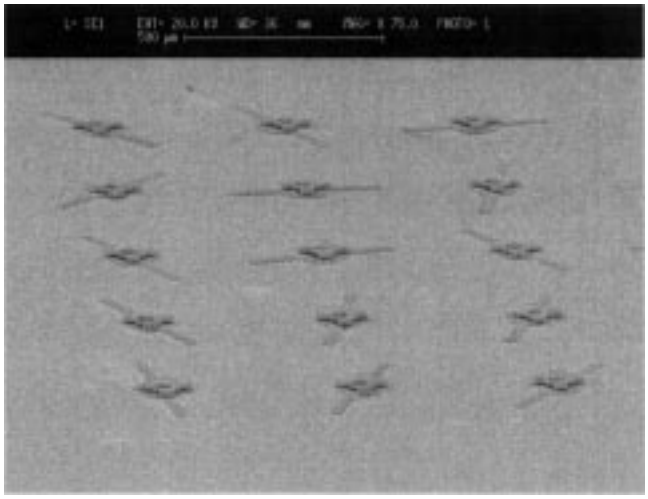

(b)

Fig. 4. SEM micrographs showing the perspective view of a microstirrer and an array. (a) A single microstirrer. Insert: a 0.5-μm gap between the rotor and the surface is created by a spacer. (b) A 5×3 mixer array.

In order to fabricate microchannels into PDMS we used micromolding methods. The channel design is first made in a piece of $\langle 100 \rangle$-oriented silicon wafer using KOH wet etching to the desired depth. PDMS is then poured onto the Si mold, cured and peeled off the mold. At the final step, the PDMS piece is aligned and bonded to the mixer wafer using a contact aligner (Karl Suss MJB-3). With the same method, a PDMS vessel with a diameter of 2.5 mm is also made, aligned and bonded to a 3×3 mixer array for the experiment of mixing in chamber.

V. Simulation

Simulation can provide insight into the complexity of microscale fluid mechanics. We believe that the design of the mixing system can be accelerated when proper computer simulation is used, to predict the trend of the behavior involved if not to accurately capture full details of microscale fluid physics. In this paper, the CFD-ACE (Version 6.4, CFD Research Corporation, Huntsville, AL) general-purpose fluid dynamics code was used to aid our design and corroborate experimental findings. The software solved the Navier-Stokes equations and the Fick's law of diffusion in order to find the fluid dynamics and homogenization of the mixture concentrations.

Two types of fluid systems were modeled. One consists of a three-dimensional fluid channel with a single microstirrer. Another model consists of a microfluid chamber with an array of mixers. The stirrer is based on an inherent implemented fan-model. In this model, the forces generated by the rotating stirrer were simply simulated as source terms to the axial and circumferential momentum equations [30]. Two fluid components (colored orange and blue) were assumed to have fluid properties identical to those of water and their initial concentrations were both 0.01 in water. The final mixture, represented by green color, therefore consisted of 0.05 orange dye, 0.05 blue dye and 0.99 water.

A. Mixing in Channel

The channel mixing was simulated as two parallel color liquids flowing through a $750 \times 70 \times 7000$ μm straight channel. The mixer was located 1000 μm away from the adjoining inlets. The pressure of the inlets was kept at a constant of 2.5 N/m^2 higher than the pressure of the outlet, resulting in a flow velocity of 140 μm/s. Simulations of channel mixing at various stirring speeds were performed.

Fig. 5 shows steady-state simulation results at different speeds of rotation. When the mixer was off, the liquids in channel were only mixed by molecular diffusion. Therefore, as shown in Fig. 5(a), the mixing occurred along the interface to a minimal extent. Results of mixing at mixer rotation speeds of 300 rpm and 600 rpm are shown in Fig. 5(b) and 5(c), respectively. Bulk motions were clearly generated in the region of the mixer. In addition, in Fig. 5(c), the streamlines (white arrows in the graphs) showed that circulation loops were formed around the mixer but did not extend to the sidewalls. Complete mixing was obtained within the diameter of the mixer.

The rotating mixer has a volume of $V = 4 \times 10^{-14}$ m^3. The mass of the rotor is 3.2×10^{-10} kg using a density of 8000 kg/m^3 for NiFe. The maximum magnitude of the magnetic torque is 7.2×10^{-11} N $\cdot$ m, occurring when the external magnetic field and the rotor are parallel to each other. The formula for estimating the mechanical torque is $T = MVH$, where H is the magnetic field intensity in air ($H = 15$ Gauss $= 1194$ A/m). The value of internal magnetization varies with respect to applied magnetic field [27]. For first-order estimation, we assume the flux intensity (or internal magnetization, M) of the rotor is constant (1.5 Tesla).

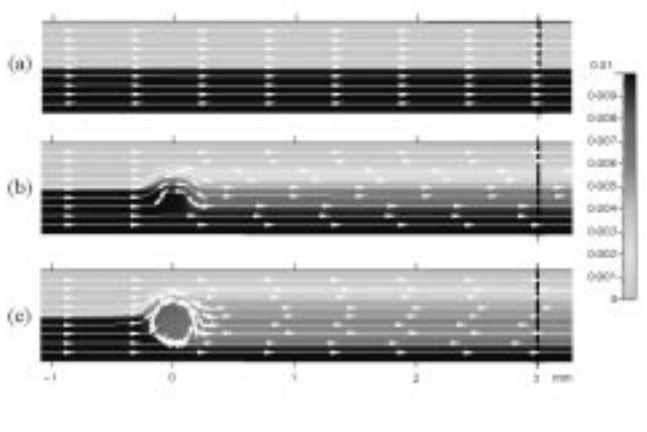

Fig. 5. CFD simulations of the channel mixing. Two dyed liquids flowing from left ($d > 0$) to right with initial concentrations of 1% are mixed by a single mixer at $d = 0$ mm.

B. Mixing in Chamber

To determine the feasibility of mixing in a chamber, a set of simulations were performed as follows. In the chamber mixing simulation, a 3×3 mixer array was placed in the middle of a $2000 \times 2000 \times 50$ μm square chamber. The spacing between the stirrers was 500 μm. After the two color dyes filled in, the liquids in chamber were still and isolated. When the microstirrers were rotating counterclockwise at 600 rpm, the fluids in the chamber started to blend and disperse to the sidewalls. Transient solutions at six time intervals are shown in Fig. 6. Successful mixing was achieved after 60 s as shown in Fig. 6(f).

VI. Experimental Investigation

The setup used to perform the mixing experiment is schematically represented in Fig. 7. The channel was filled with DI water by suction force using a plastic syringe. The rotor is activated using the rotating magnet in a commercial hotplate/stirrer (Cole-Parmer Inc., Vernon Hills, IL). The hotplate is capable of providing an external rotating magnetic field. The maximum magnetic field intensity measured at the micromixer plane is 15 Gauss.

It is important to determine whether the rotor speed corresponds to the speed of the rotating external magnet. Operation of mixers was examined *in situ* using a laser-detector configuration. Specifically, we calibrated the rotation speed of the micromixer as a function of the macromagnetic bar in the hotplate. A 670-nm-wavelength, 0.5-mm-diameter laser beam (LDM145, Edmund Industrial Optics, Barrington, NJ) was reflected off the substrate and collected by a phototransistor (L14G2, Fairchild Semiconductor). The rotation of the bar causes light to be pe-

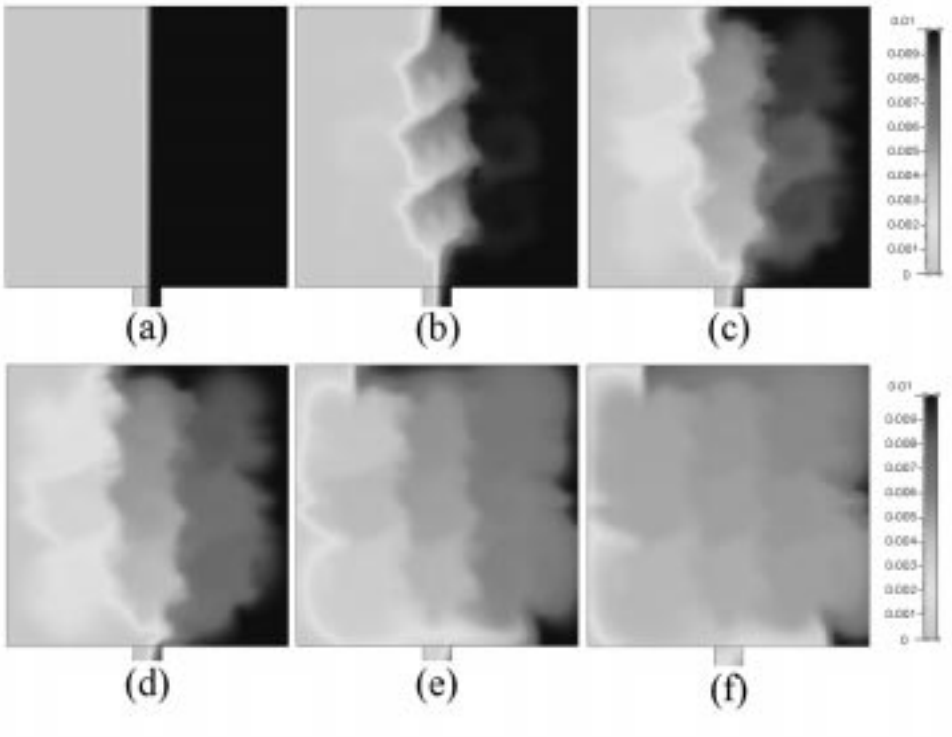

Fig. 6. Simulation of array mixing sequences in a $2000 \times 2000 \times 50\,\mu$m microfluid chamber with a 3×3 array of mixers each rotating at 600 rpm. (a) No mixing occurs when the chamber is initially filled with two fluids. (b)–(f) The distribution of color at $t = 1$ s, 5 s, 10 s, 30 s and 60 s, respectively.

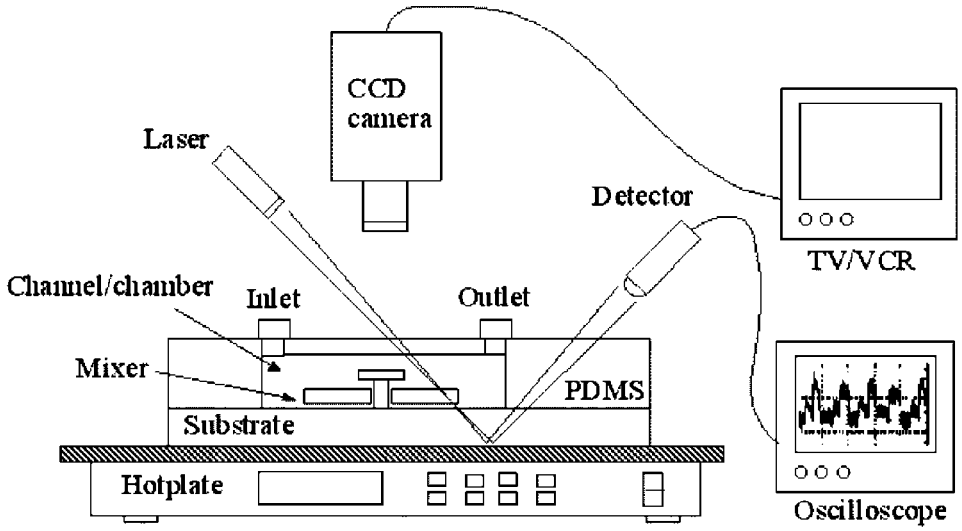

Fig. 7. Schematic representation of the experimental setup used for characterizing the mixing results and validating the rotor speed.

riodically blocked. This periodic output signal from the photodiode formed a pulse train at the frequency of $2N$, where N is the rotating speed of the rotor in the unit of rpm. The measured rotor speed as a function of the input (as indicated by the hotplate instrument) is shown in Fig. 8. At low rotation speed, e.g., lower than 100 rpm, the magnetic rotor speed is unstable. Further, at speeds above 600 rpm, the hotplate starts to vibrate significantly, preventing measurements to be made. As a consequence, the measurement is conducted between 300–600 rpm. This test verifies that mixers can rotate smoothly in this microfluidic system and synchronize with the magnetic field of the hotplate. Consequently, the rotating speed of the mixer mentioned in the following text refers to stirring speed of the magnetic bar in the hotplate unless noted otherwise.

Mixing is usually evaluated by visualization methods using fluorescent dyes [6], [9], [13], [15], [16], pH indicators [20], [31] and color dyes [19], [32]. In this paper, we use food color dyes (orange and blue colored) for their simplicity and high contrast. Fluorescent dyes are not suitable because the hotplate/stirrer could not be fitted into a fluorescence microscope. Future modification is planned.

Video images taken with a CCD camera (SONY Electronics Inc., Park Ridge, NJ) are converted into sequential 640×480 TIFF-formatted graphs with an image capture card (DVC II,

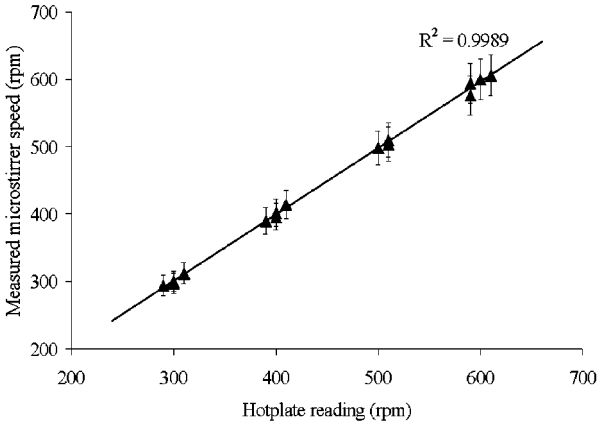

Fig. 8. The measured rotating speed of the mixer at various stirring rates of the magnet in the commercial hotplate. A linear relation is observed up to 600 rpm, when the hotplate self-vibration prevents further accurate optical and fluid measurement.

Dazzle, Inc., Fremont, CA). The spatial-temporal variation of color in the fluid channel is analyzed using an image-analysis software (Scion Image, Scion Co., Frederick, MD). The 24-bit indexed color of each pixel is converted into a three-slice RGB stack, of which the red slice is used to build the monotone spectrum. For example, the index of color at a given pixel (denoted c) is 0 for red and 255 for black. By this process, the actual color index of the orange and blue mixture spans from 88 to 231.

The image analysis software is capable of extracting data along a defined line or over a certain area. To quantify the mixing results statistically, a mixing index is defined as the standard derivation of color index at individual pixels [9]

$$\text{Mixing index} = \sqrt{\frac{1}{N}\sum\left(\frac{c_k - \bar{c}}{\bar{c}}\right)^2}. \qquad (2)$$

The term c_k is the color index at a pixel k and $\bar{c}$ is the average over N pixels along a sampling line or over a sampling area. The more uniform the mixture is, the smaller the mixing index becomes. Accordingly, we can compare mixing indexes in the channel flow at different cross sections and calculate the mixing time required in a stirred chamber.

A. Mixing in a Channel

Fig. 9 shows mixing of two colored fluids in a 750-μm-wide and 70-μm-deep channel with a single stirrer positioned at the junction. First, the channel and the reservoirs were filled with DI water. Equal amounts of blue- and orange-colored dyes (5 μl) were injected to inlet reservoirs using a microliter syringe (Hamilton Company, Reno, NV). This generated a pressure flow (with a flow rate of 0.17 μl/min) that brought the dyed liquids downstream to the outlet reservoir. Due to low Reynolds number, the extent of mixing was limited by slow diffusion and hence the channel was divided into two color regions, as shown in Fig. 9(a). When the rotor started to rotate, it exerted forces on the fluid, causing a localized circular motion of fluid particles. Fluids in this region were mixed within a few cycles [see Fig. 9(b) and (c)].

Similar to the case observed in the simulation, it can be seen that the mix did not disperse effectively to the sidewalls. Consequently, we measure the mixing index only in the area of interest, as marked by white lines in Fig. 9(c). The mixing index at different locations is obtained according to (2) by averaging over sampling lines located at a distance d from the center of the rotor.

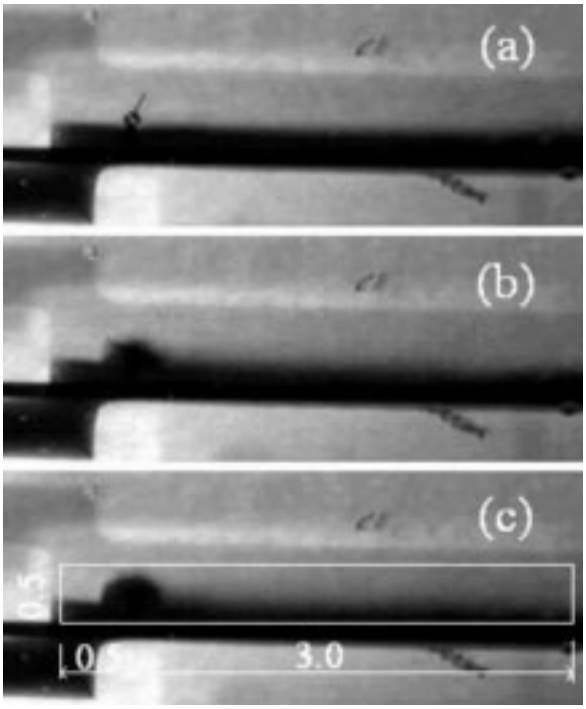

Fig. 9. Captured video frames showing channel mixing with a single microstirrer ($d = 0$) at (a) rest, (b) 150 rpm and (c) 300 rpm. The marked region is the area of interest. Unit: mm.

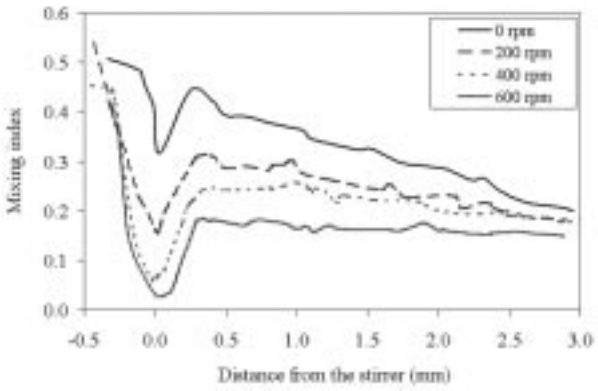

Fig. 10. The mixing index at different distance d and under various rotor speeds. Mixing efficiency is improved with a higher stirring speed. The distance between each pixel is 6.25 μm. The mixing index is a coefficient of variation over the 0.4-mm length transverse to the flow.

The mixing index is related to both the location in the channel and the rotation speed of the rotor. Fig. 10 shows the mixing index measured at sampling lines along the channel length with different speeds of rotation. The rotor speeds are 0, 200, 400 and 600 rpm. In each case, the mixing index decreases as the fluid moves downstream. Without the stirring effect (i.e., rotor speed equals zero), the mixing index was above 0.2 until it was 3 mm downstream. Note that a sudden dip near the stirrer was

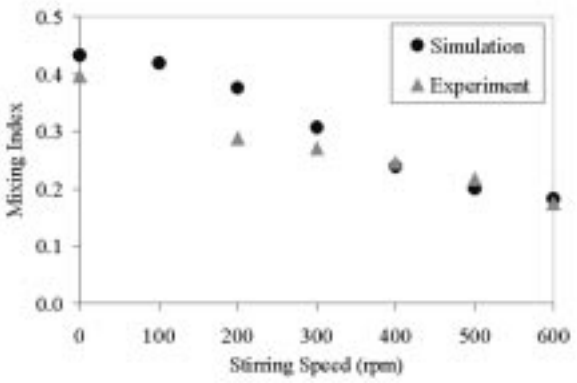

Fig. 11. Comparison of experimental data and simulations of channel mixing. The mixing index is measured at $d = 0.5$ mm.

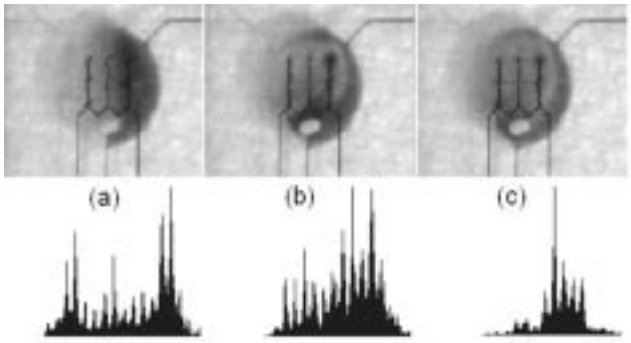

Fig. 12. Top: Grabbed sequential video frames of mixing in a 2.5 mm-diameter chamber by an array (3×3) of stirrers each rotating at 600 rpm. Results at (a) 0 s, (b) 30 s and (c) 60 s. Bottom: Color histogram corresponding to each case illustrated above. The histogram curve becomes narrower as the mixing action causes the color in the chamber to become uniform.

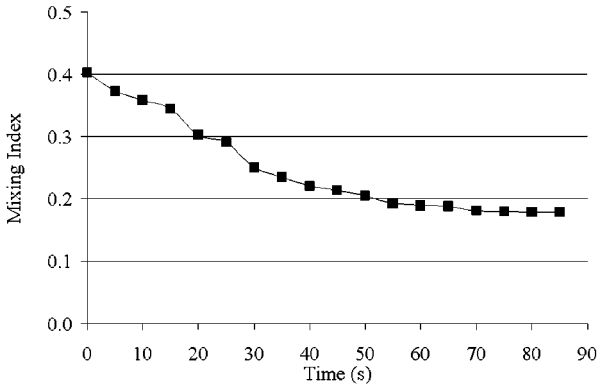

Fig. 13. Mixing index versus time in the reaction chamber. The mixing index is measured over a 2.5-mm-diameter circle (17503 pixels). Complete mixing (mixing index < 0.2) is achieved after 55 s in a large reaction chamber.

believed to be due to the color of the rotor itself. When the rotor speed is nonzero, the mixing index is significantly lower near the rotor than that at the start. This drop is beyond the artifact introduced by the color of the rotor itself. When the stirring speed was 600 rpm, the mixing index dropped to 0.18 as soon as it passed the stirrer. The effect of enhanced mixing is confirmed at each of the rotor speeds tested.

Also from the graph we conclude that the mixing improves with increased rotor speed. Since we were unable to test rotor speeds below 100 rpm or beyond 600 rpm, the continuation of this trend is only concluded within the range of rotor speeds tested.

Fig. 9 shows that the mixing effect in a channel does not extend significantly beyond the region defined by the diameter of the rotor. The mixing seems to be confined by the diameter of the rotor itself. There are several possible solutions and improvements to the design. First, the width of the channel and the diameter of the rotor should match in future designs in order to create full-channel-width mixing. Second, we plan to design rotors with angled portions at two ends to drive fluid particles in the axial direction. This could potentially increase the mixing in regions beyond the diameter of the rotor.

Fig. 11 compares the experimental result with the simulation of the channel mixing at $d = 0.5$ mm. The mixing index for the simulation case is obtained by averaging the concentration rather than color index. The formula used is similar to (2), with the color index terms being replaced by concentration terms. It can be seen that the simulation predicts accurately that the mixing effectiveness is dependent on the rotor speed and that the mixing index becomes less than 0.2 at high stirring speed.

B. Mixing in a Chamber

Microscale mixing in a flow-through configuration is the most commonly used technique nowadays. However, for certain sequential analysis applications the mixing is required to take place in a larger reaction chamber. We have demonstrated that an array of micromixers operating simultaneously is capable of providing effective mixing in a large reaction chamber. Fig. 12 demonstrates mixing in a chamber with a diameter of 2.5 mm and a height of 40 μm, using a 3×3 microstirrer array, each operating at 600-rpm rotation speed. The color histogram was measured over a 2.5-mm-diameter circle (17503 pixels). The mixing caused the color in the chamber to become more uniformly distributed, resulting in increasingly narrower peaks in the color histogram. The mixing index of the chamber was also measured over the same area. Full mixing (i.e., defined as mixing index < 0.2) is achieved in 55 s as shown in Fig. 13 and the results correspond well to the simulation results.

VII. Conclusion

We have presented the design and fabrication of a microstirrer and its array for microfluid mixing. The mixers are actuated remotely by a rotating magnetic field. Microscale mixing in a channel and sequential mixing in a chamber have been successfully demonstrated. We found that the mixing efficiency can be enhanced by increasing the stirring speed. Rapid mixing in a large chamber was also shown with a 3×3 mixer array. Simulation models have been built using commercially available software. The simulations provided guidance to our design.

Acknowledgment

The authors would like to thank R. Blaney and J. Hughes for maintaining the microfabrication facility in the Microelectronics Laboratory of the University of Illinois.

REFERENCES

[1] K. F. Jensen, "The impact of MEMS on the chemical and pharmaceutical industrials," in *Proc. IEEE Sens. and Actuator Workshop*, Hilton Head Island, SC, June 2000, pp. 105–110.

[2] C.-M. Ho, "Fluidics—The link between micro and nano sciences and technologies," in *Proc. IEEE MEMS Workshop*, Interlaken, Switzerland, January 2001, pp. 375–384.

[3] H. Chaté and E. Villermaux, *Mixing Chaos and Turbulence*, J.-M. Chomez, Ed. New York: Kluwer Academic/Plenum Publishers, 1996, pp. 37–56.

[4] J. B. Knight, A. Vishwanath, J. P. Brody, and R. H. Austin, "Hydrodynamic focusing on a silicon chop: Mixing nanoliters in microseconds," *Phys. Rev. Lett.*, vol. 80, no. 17, pp. 3863–3866, April 1998.

[5] R. Miyake, T. S. J. Lammerink, M. Elwenspoek, and J. H. J. Fluitaman, "Micro mixer with fast diffusion," in *Proc. 7th Int. Conf. Solid-State Sens. and Actuators*, 1993, pp. 248–253.

[6] J. Branebjerg, P. Gravesen, J. P. Krog, and C. R. Nielsen, "Fast mixing by lamination," in *Proc. IEEE MEMS Workshop*, San Diego, CA, 1996, pp. 441–446.

[7] N. Schwesinger, T. Frank, and H. Wurmus, "A modular microfluid system with an integrated micromixer," *J. Micromech. Microeng.*, vol. 6, pp. 99–102, 1996.

[8] W. Ehrfeld, K. Golbig, V. Hessel, H. Lowe, and T. Richter, "Characterization of mixing in micromixer by a test reaction: Single mixing units and mixer arrays," *Ind. Eng. Chem. Res.*, vol. 38, pp. 1075–1082, 1999.

[9] J. M. Ottino, *The Kinematics of Mixing: Stretching, Chaos and Transport*. New York: Cambridge University Press, 1989.

[10] R. H. Liu *et al.*, "Passive mixing in a three-dimensional serpentine microchannel," *J. Microelectromech. Syst.*, vol. 9, pp. 190–197, June 2000.

[11] A. Bertsch, S. Heimgartner, P. Cousseau, and P. Renaud, "3D micromixers—Downscaling large scale industrial static mixers," in *Proc. IEEE MEMS Workshop*, Interlaken, Switzerland, Jan. 2001, pp. 507–510.

[12] A. D. Stroock, S. K. W. Dertinger, A. Ajdari, I. Mezic, H. A. Stone, and G. M. Whitesides, "Chaotic mixer for micro channels," *Science*, vol. 295, no. 5555, pp. 647–651, 2001.

[13] J. W. Choi and C. H. Ahn, "An active micro mixer using electrohydrodynamic (EHD) convection," in *Proc. Solid-State Sens. and Actuator Workshop*, Hilton Head Island, SC, June 2000, pp. 52–55.

[14] M. Volpert, C. D. Meinhart, I. Mezic, and M. Dahelh, "An actively controlled micromixer," in *Proc. MEMS, ASME IMECE*, Nashville, TN, 1999, pp. 483–48.

[15] J. Voldman, M. L. Gary, and M. A. Schimdt, "An integrated liquid mixer/valve," *J. Microelectromech. Syst.*, vol. 9, no. 3, pp. 295–302, Sept. 2000.

[16] K. Hosokawa, T. Fujii, and I. Endo, "Droplet-based nano/picoliter mixer using hydrophobic microcapillary vent," in *Proc. IEEE MEMS Workshop*, Orlando, FL, 1999, pp. 388–393.

[17] A. A. Deshmukh, D. Liepmann, and A. P. Pisano, "Characterization of a micro-mixing, pumping and valving system," in *Proc. 11th Int. Solid-State Sens. and Actuators*, Munich, Germany, 2001, pp. 950–953.

[18] R. M. Moroney, R. M. White, and R. T. Howe, "Ultrasonically induced microtransport," in *Proc. IEEE MEMS Workshop*, Nara, Japan, 1991, pp. 277–282.

[19] Z. Yang, H. Goto, M. Matsumoto, and R. Maeda, "Ultrasonic micromixer for microfluidic systems," in *Proc. 13th Annual Int. Conference on Micro Electro Mechanical Systems*, Miyazaki, Japan, Jan. 2000, pp. 80–85.

[20] X. Zhu and E. S. Kim, "Microfluidic motion generation with acoustic waves," *Sens. Actuators, A. Phys.*, vol. 66, no. 1–3, pp. 355–360, Apr. 1998.

[21] P. Woias, K. Hauser, and E. Yacoub-George, "An active silicon micromixer for μTAS application," in *Proc. Micro Total Analysis Systems Symp.*, Enschede, The Netherlands, 2000, pp. 277–282.

[22] J. Evans, D. Liepmann, and A. P. Pisano, "Planar laminar mixer," in *Proc. IEEE MEMS Workshop*, 1997, pp. 96–101.

[23] J.-H. Tsai and L. Lin, "Thermal bubble powered microfluidic mixer with gas bubble filter," in *Proc. 11th Int. Solid-State Sens. and Actuators*, Munich, Germany, 2001, pp. 966–969.

[24] D. J. Beebe, G. Mensing, J. Moorthy, C. M. Khoury, and T. M. Pearce, "Alternative approaches to microfluidic systems design, construction and operation," in *Proc. Micro Total Analysis Systems (μTAS 2001) Symposium*, Monterey, CA, 2001, pp. 453–455.

[25] H. Suzuki and C. M. Ho, "A magnetic force driven chaotic micro-mixer," in *Proc. 15th Int. Conf. on Micro Electro Mechanical Systems, MEMS'02*, Las Vegas, NV, 2002, pp. 40–43.

[26] Y.-K. Lee, J. Deval, P. Tabeling, and C.-M. Ho, "Chaotic mixing in electrokinetically and pressure driven micro flow," in *Proc. IEEE MEMS Workshop*, Interlaken, Switzerland, Jan. 2001, pp. 483–486.

[27] J. W. Judy, R. S. Muller, and H. H. Zappe, "Magnetic microactuation of polysilicon flexure structures," *J. Microelectromechan. Syst.*, vol. 4, pp. 162–169, 1995.

[28] A. W. Patwardhan and J. Joshi, "Relation between flow pattern and blending in stirred tanks," *Ind. Eng. Chem. Research*, vol. 38, pp. 3131–3143, 1999.

[29] P. F. Man, D. K. Jones, and C. H. Mastrangelo, "Microfluidic plastic capillaries on silicon substrates: A new inexpensive technology for bioanalysis chips," in *Proc. IEEE MEMS Workshop (MEMS '97)*, Jan. 1997, pp. 311–316.

[30] *CFD-ACE (U) User Manual*, CFD Research Corporation, 2000.

[31] A. Desai, D. Bökenkamp, X. Yang, Y.-C. Tai, E. Marzluff, and S. Mayo, "Microfluidic sub-millisecond mixers for the study of chemical reaction kinetics," in *Proc. 9th Int. Solid-State Sens. and Actuators (Transducer '97)*, vol. 1, Chicago, IL, June 1997, pp. 167–170.

[32] R. U. Seidel, D. Y. Si, W. Menz, and M. Esashi, "Capillary force mixing device as sampling module for chemical analysis," in *Proc. 10th Int. Conf. Solid-State Sens. and Actuators (Transducers '99)*, Sendai, Japan, June 1999, pp. 438–441.

Liang-Hsuan Lu received the B.S. degree from the National Taiwan University, Taiwan, and the M.S. degree in microfluidics systems from the University of Illinois, Urbana, in January of 2002.

He is currently residing in Taipei, Taiwan.

Kee Suk Ryu received the B.S. degree in mechanical engineering from the Hanyang University, Seoul, Korea, and the M.S. degree in bioengineering from the Georgia Institute of Technology, Atlanta. He is currently pursuing the Ph.D. degree at the Micro Actuators, Sensors and Systems group of the University of Illinois, Urbana.

His research interests are in the area of MEMS with focus on microfluidics and BioMEMS.

Chang Liu received the M.S. and Ph.D. degree from the Micromachining Group of the California Institute of Technology (Caltech), Pasadena, in 1991 and 1996, respectively.

Currently, he is an Assistant Professor at the University of Illinois, Urbana. His research interests include microfluid systems for biochemical analysis, the application of MEMS in nanotechnology and microintegrated sensors (including biomimetic sensors). His group website is http://mass.micro.uiuc.edu